which may be subject to bias (*37*, *38*). Fifth, we do not measure health outcomes in this demand study, but combining our results on reductions in OD with studies that measure the relationship between OD and health outcomes (*14*, *39*–*41*) suggests that sanitation marketing interventions could plausibly produce improvements in health. Finally, the scale of this study, covering over 18,000 households and 100% samples of four subdistricts, allows us to document some of the general equilibrium changes operating via a social influence mechanism, but our results remain silent on wider general equilibrium effects operating via price mechanisms.

REFERENCES AND NOTES

1. WHO/UNICEF, "Progress on Drinking Water and Sanitation - 2014 Update," tech. rep. (WHO/UNICEF Joint Monitoring Programme for Water Supply and Sanitation, Luxembourg, 2014). URL (accessed 9 April 2015): http://apps.who.int/iris/bitstream/10665/112727/1/9789241507240_eng.pdf?ua=1.
2. A. Prüss-Ustün *et al.*, *Trop. Med. Int. Health* **19**, 894–905 (2014).
3. A. D. Dangour *et al.*, *Cochrane Database Syst. Rev.* **8**, CD009382 (2013).
4. A. Lin *et al.*, *Am. J. Trop. Med. Hyg.* **89**, 130–137 (2013).
5. D. Spears, A. Ghosh, O. Cumming, *PLOS ONE* **8**, e73784 (2013).
6. World Bank WSP, "Water and Sanitation End of Year Report Fiscal Year 2013", tech. rep. (World Bank Water and Sanitation Program, Washington, DC, 2013). URL (accessed 9 April 2015): https://wsp.org/sites/wsp.org/files/publications/WSP-End-Year-Report-FY13.pdf.
7. Census Organization of India, *15th Indian Census - Houses, Household Amenities and Assets: Sanitation - Total Latrine Table*, 2011. URL (accessed 9 April 2015): www.devinfolive.info/censusinfodashboard/website/index.php/pages/sanitation/total/Households/IND.
8. S. Mojumdar, *Untitled Memorandum, no. W-11042/34/2014-NBA* (July 2014). URL (accessed 9 April 2015): www.mdws.gov.in/sites/upload_files/ddws/files/pdf/Swachh_Bharat_by_2019.pdf.
9. S. Prasad, *Swachchh Bharat by 2019* (July 2014). URL (accessed 9 April 2015): http://mdws.gov.in/hindi/sites/upload_files/ddwshindi/files/Swachchh_Bharat_by_2019.pdf.
10. Press Trust of India, "Modi's new mantra: Toilets first, temples later," *Hindustan Times* (October 2013). URL (accessed 9 April 2015): www.hindustantimes.com/newdelhi/modi-s-new-mantra-toilets-first-temples-later/article1-1130281.aspx.
11. E. Perez *et al.*, "What Does It Take to Scale Up Rural Sanitation?" Water and Sanitation Program Working Paper (July 2012). URL (accessed 9 April 2015): www.wsp.org/sites/wsp.org/files/publications/WSP-What-does-it-take-to-scale-up-rural-sanitation.pdf.
12. K. Kar, K. Pasteur, "Subsidy or self-respect?: Community led total sanitation; an update on recent developments," IDS Working Paper 257 (Institute of Development Studies, University of Sussex, Brighton, UK, 2005).
13. K. Kar, "Subsidy or self-respect? Participatory total community sanitation in Bangladesh." IDS Working Paper 184 (Institute of Development Studies, University of Sussex, Brighton, UK, 2003).
14. D. Spears, *Effects of Rural Sanitation on Infant Mortality and Human Capital: Evidence from India's Total Sanitation Campaign* (July 2012). URL (accessed 9 April 2015): www.dartmouth.edu/~neudc2012/docs/paper_86.pdf.
15. A. Hueso, B. Bell, *Water Policy* **15**, 1001–1017 (2013).
16. S. Barnard *et al.*, *PLOS ONE* **8**, e71438 (2013).
17. S. R. Patil *et al.*, *PLOS Med.* **11**, e1001709 (2014).
18. S. Trémolet, "Sanitation Markets: Using economics to improve the delivery of services along the sanitation value chain," tech. rep. (SHARE, London, UK, December 2012). URL (accessed 9 April 2015): www.shareresearch.org/LocalResources/SHARE_sanitation_markets_pathfinder_Dec_2012.pdf.
19. Materials and Methods, section S1.2.
20. R. Sigler, L. Mahmoudi, J. P. Graham, *Health Promot. Int.* **30**, 16–28 (2015).
21. Materials and methods, section S1.6.
22. S. Hanchett, M. H. Khan, L. Krieger, C. Kullmann, paper presented at the 35th WEDC International conference, "The future of water sanitation and hygiene: Innovation, adaptation and engagement in a changing world," Loughborough, UK, 2011. URL (accessed 9 April 2015): http://wedc.lboro.ac.uk/resources/conference/35/Hanchett-S-1036.pdf.
23. Materials and methods, section S1.5.
24. D. Mara, J. Lane, B. Scott, D. Trouba, *PLOS Med.* **7**, e1000363 (2010).
25. Effects on ineligibles discussed in the supplementary text, section S2.2.
26. Details in tables S2 and S3.
27. Supplementary text, section S2.1.
28. Details, including effects on access, in tables S4 and S5.
29. A. Ahuja, M. Kremer, A. P. Zwane, *Annu. Rev. Resour. Econ.* **2**, 237–256 (2010).
30. P. Dupas, *Science* **345**, 1279–1281 (2014).
31. A. M. Mobarak, P. Dwivedi, R. Bailis, L. Hildemann, G. Miller, *Proc. Natl. Acad. Sci. U.S.A.* **109**, 10815–10820 (2012).
32. Supplementary text, section S2.2.
33. K. Dickinson, S. K. Pattanayak, "Open sky latrines: Do social effects influence technology adoption in the case of a (very) impure public good?" (2009). URL (accessed 9 April 2015): www.isid.ac.in/~pu/conference/dec_09_conf/Papers/SubhrenduPattanayak.pdf.
34. S. K. Pattanayak *et al.*, *Bull. World Health Org.* **87**, 580–587 (2009).
35. A. Banerjee, A. G. Chandrasekhar, E. Duflo, M. O. Jackson, *Science* **341**, 1236498 (2013).
36. D. Spears, "How Much International Variation in Child Height Can Sanitation Explain?" Working Paper 6351 (World Bank Policy Research, 2013). URL (accessed 9 April 2015): www-wds.worldbank.org/external/default/WDSContentServer/IW3P/IB/2013/02/05/000158349_20130205082533/Rendered/PDF/wps6351.pdf.
37. T. Clasen *et al.*, *Environ. Sci. Technol.* **46**, 3295–3303 (2012).
38. M. W. Jenkins, M. C. Freeman, P. Routray, *Int. J. Environ. Res. Public Health* **11**, 8319–8346 (2014).
39. D. Coffey, "Sanitation externalities, disease, and children's anemia," Working Paper (Princeton University, March 2014). URL (accessed 9 April 2015): http://paa2014.princeton.edu/papers/140309.
40. M. Geruso, D. Spears, "Neighborhood Sanitation and Infant Mortality," Working Paper (RICE Institute, January 2015). URL (accessed 9 April 2015): www.amse-aixmarseille.fr/sites/default/files/_evenements/muslim_v2.pdf.
41. D. Spears, S. Lamba,"Effects of Early-Life Exposure to Sanitation on Childhood Cognitive Skills" (The World Bank Sustainable Development Network Water and Sanitation Program Unit, October 2013, Working Paper 6659). URL (accessed 9 April 2015): http://elibrary.worldbank.org/doi/pdf/10.1596/1813-9450-6659

ACKNOWLEDGMENTS

We are grateful to WaterAid Bangladesh and VERC for implementing the interventions and Innovations for Poverty Action for assistance running the study. We also thank the study participants for generously giving their time, as well as the field officers for their dedication to the quality of data collected. I. Ahmed, M. Ali, B. Atuesta, M. Bakhtiar, Z. Chen, L. Feeney, M. Khan, R. Mahbub, A. Moderson-Kox, L. Moore, A. Vargas, D. Wolfson, and T. Zelenska provided excellent project management and research assistance. We thank The Bill and Melinda Gates Foundation (BMGF) for generous funding. BMGF, WaterAid Bangladesh, and VERC were involved in the study design but played no role in data collection, analysis, the decision to publish, or manuscript preparation. The activities associated with this research were approved by the Yale University Human Subject Committee Protocol no. 1203009864. The authors declare no conflicts of interest. Data and replication code are publicly available at the Harvard Dataverse Network (doi:10.7910/DVN/GJDUTV).

SUPPLEMENTARY MATERIALS

www.sciencemag.org/content/348/6237/903/suppl/DC1
Materials and Methods
Supplementary Text
Figs. S1 to S7
Tables S1 to S9

10 October 2014; accepted 7 April 2015
Published online 16 April 2015;
10.1126/science.aaa0491

NEUROPHYSIOLOGY

Decoding motor imagery from the posterior parietal cortex of a tetraplegic human

Tyson Aflalo,[1]* Spencer Kellis,[1]* Christian Klaes,[1] Brian Lee,[2] Ying Shi,[1] Kelsie Pejsa,[1] Kathleen Shanfield,[3] Stephanie Hayes-Jackson,[3] Mindy Aisen,[3] Christi Heck,[2] Charles Liu,[2] Richard A. Andersen[1]†

Nonhuman primate and human studies have suggested that populations of neurons in the posterior parietal cortex (PPC) may represent high-level aspects of action planning that can be used to control external devices as part of a brain-machine interface. However, there is no direct neuron-recording evidence that human PPC is involved in action planning, and the suitability of these signals for neuroprosthetic control has not been tested. We recorded neural population activity with arrays of microelectrodes implanted in the PPC of a tetraplegic subject. Motor imagery could be decoded from these neural populations, including imagined goals, trajectories, and types of movement. These findings indicate that the PPC of humans represents high-level, cognitive aspects of action and that the PPC can be a rich source for cognitive control signals for neural prosthetics that assist paralyzed patients.

The posterior parietal cortex (PPC) in humans and nonhuman primates (NHPs) is situated between sensory and motor cortices and is involved in high-level aspects of motor behavior (*1*, *2*). Lesions to this region do not produce motor weakness or primary sensory deficits but rather more complex sensorimotor losses, including deficits in the rehearsal of movements (i.e., motor imagery) (*3*–*7*). The activity of PPC neurons recorded in NHPs reflects

the movement plans of the animals, and they can generate these signals to control cursors on computer screens without making any movements (*8*–*10*). It is tempting to speculate that the animals have learned to use motor imagery for this "brain control" task, but it is of course not possible to ask the animals directly. These brain control results are promising for neural prosthetics because imagined movements would be a versatile and intuitive method for controlling external devices (*11*). We find that motor imagery recorded from populations of human PPC neurons can be used to control the trajectories and goals of a robotic limb or computer cursor. Also, the activity is often specific for the imagined effector (right or left limb), which holds promise for bimanual control of robotic limbs.

A 32-year-old tetraplegic subject, EGS, was implanted with two microelectrode arrays on 17 April 2013. He had a complete lesion of the spinal cord at cervical level C3-4, sustained 10 years earlier, with paralysis of all limbs. Using functional magnetic resonance imaging (fMRI), we asked EGS to imagine reaching and grasping. These imagined movements activated separate regions of the left hemisphere of the PPC (fig. S1). A reach area on the superior parietal lobule (putative human area 5d) and a grasp area at the junction of the intraparietal and postcentral sulci (putative human anterior intraparietal area, AIP) were chosen for implantation of 96-channel electrode arrays. Recordings were made over more than 21 months with no adverse events related to the implanted devices. Spike activity was recorded and used to control external devices, including a 17–degree-of-freedom robotic limb and a cursor in two dimensions (2D) or 3D on a computer screen.

Recordings began 16 days after implantation. The subject could control the activity of single cells through imagining particular actions. An example of volitional control is shown in movie S1. The cell is activated when EGS imagines moving his hand to his mouth but not for movements with similar gross characteristics such as imagined movements of the hand to the chin or ear. Another example (movie S2) shows EGS increasing the activity of a different cell by imagining rotation of his shoulder, and decreasing activity by imagining touching his nose. In many cases, the subject could exert volitional control of single neurons by imagining simple movements of the upper arm, elbow, wrist, or hand.

We found that EGS's neurons coded both the goal and imagined trajectory of movements. To characterize these forms of spatial tuning, we used a masked memory reach paradigm (MMR, Fig. 1A). In the task, EGS imagined a continuous reaching movement to a spatially cued target after a delay period during which the goal was removed from the screen. On some trials, motion

[1]Division of Biology and Biological Engineering, California Institute of Technology, Pasadena, CA 91125, USA. [2]USC Neurorestoration Center and the Departments of Neurosurgery and Neurology, University of Southern California, Los Angeles, CA 90033, USA. [3]Rancho Los Amigos National Rehabilitation Center, Downey, CA 90242, USA.
*These authors contributed equally to this work. †Corresponding author. E-mail: andersen@vis.caltech.edu

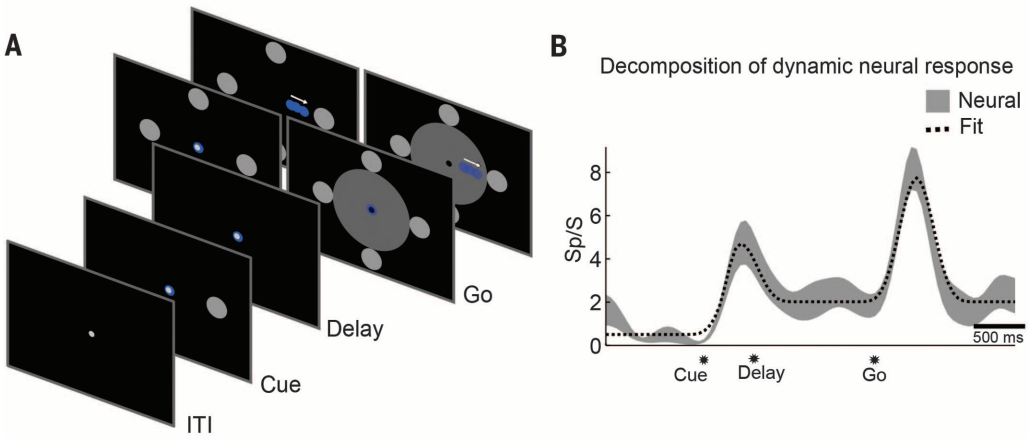

Fig. 1. Goal and trajectory coding in the PPC. (**A**) The masked memory reach task was used to quantify goal and trajectory tuning in the PPC by dissociating their respective tuning in time. EGS imagined a continuous reaching movement to spatially cued targets after a delay period. Motion of the cursor was occluded from view by using a mask in interleaved trials. (**B**) Goal and trajectory fitting. Average neural response (±SE) of a sample neuron over the duration of a trial, along with a linear model reconstruction of the time course. The linear model included components for the transient early visual response, sustained goal tuning, and transient trajectory tuning. The significance of the fit coefficients was used to determine population tuning to goal and trajectory (see Fig. 2).

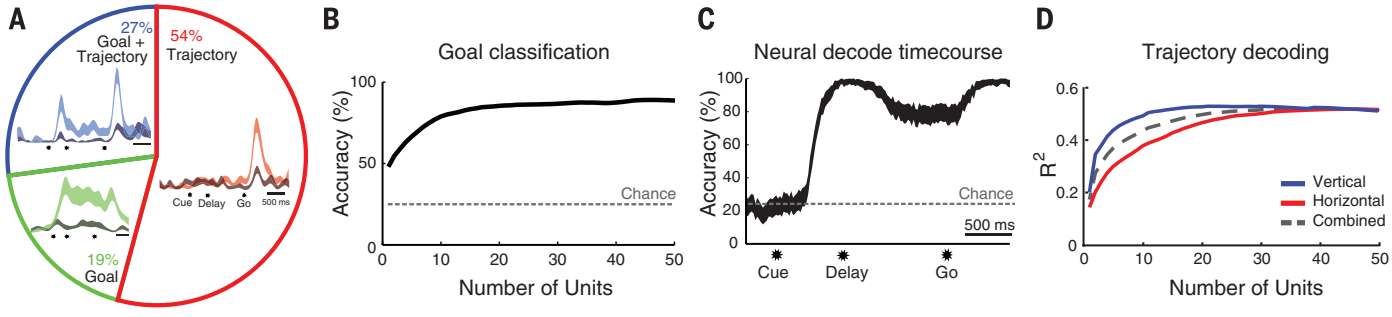

Fig. 2. Neurons in PPC encode both the goal and trajectory of movements. (**A**) The pie chart indicates the proportion of units that encode trajectory exclusively, goal exclusively, or mixed goal and trajectory. Insets show the activity (mean ± SE) for three example neurons. The lighter hue indicates response to the direction evoking maximal response; the darker hue indicates response for the opposite direction. Data taken from masked trials to avoid visual confounds (Fig. 1A). (**B**) Small populations of informative units allow accurate classification of motor goals from delay-period activity (when no visible target is present). Using a greedy algorithm, an optimized neural population for data combined across multiple days shows that >90% classification is possible with fewer than 30 units. (**C**) Temporal dynamics of goal representation. Offline analysis depicting accuracy of target classification through time [300-ms sliding window, 95% confidence interval (CI)]. Significant classification occurs within 190 ms of target presentation. (**D**) Similar to (B) but for trajectory reconstructions. All data taken from the MMR task (Fig. 1A).

of the cursor was blocked from view by using a mask. This allowed us to characterize spatial tuning for goals and trajectories (Fig. 1B) while controlling for visual confounds.

The number of recorded units was relatively constant through time, but units would appear and disappear on individual channels over the course of hours, days, or weeks (fig. S2). This allowed us to sample the functional properties of a large population of PPC neurons. From 124 spatially tuned units recorded across 7 days with the MMR task, 19% coded the goal of movement exclusively, 54% coded the trajectory of the movement exclusively, and 27% coded both goal and trajectory (Fig. 2A). Goal-tuned units supported accurate classification of spatial targets (>90% classification with as few as 30 units), representing the first known instance of decoding high-level motor intentions from human neuronal populations (Fig. 2B). The goal encoding was rapid with significant classification (shuffle test) occurring within 190 ms of cue presentation and remaining high during the delay period in which there was no visual goal present (Fig. 2C). Similarly, this population of neurons enabled reconstructions of the moment-to-moment velocity of the effector (Fig. 2D) with coefficient of determination (R^2) comparable to those reported for offline reconstructions of velocity in human M1 studies [e.g., (*12*, *13*); see also fig. S3]. In other tasks, trajectory-tuned units supported instantaneous volitional control of an anthropomorphic robotic limb at its endpoint (see movie S3).

In the MMR task, goal tuning was not directly used by the subject to control the computer interface; only the trajectory of the cursor was under brain control. To verify that goal-tuned units could support direct selection of spatial targets in closed-loop brain control, we used a direct goal classification (DGC) task (Fig. 3A). Target classification was performed by using neural activity taken during a delay period, after the visual cue was extinguished, so that neural activity was more likely to reflect intent. Online classification accuracy was significant (shuffle test); however, similar to the MMR task, aggregating neurons across days improved classification accuracy by providing a better selection of well-tuned units (Fig. 3, C and D). Goal decoding accuracy was enhanced despite the presence of more targets (six versus four) when the subject controlled the closed-loop interface using goal activity as compared to trajectory activity (Fig. 3C). Consistent with the idea that spatially tuned neural activity reflected volitional intent, decode accuracy was maintained whether the target was cued by a flashed stimulus or cued symbolically (Fig. 3, B and D).

To what degree was the spatially tuned activity specific for imagined actions of the limb? Does the activity reflect the intentions to move a specific limb, or more general spatial processes? Effector specificity was tested by asking EGS to imagine moving his left or right arm, or make actual eye movements in the symbolically cued delayed movement paradigm (Fig. 3B). We found cells that showed specificity for each effector (Fig. 4, A to C). Although the degree of specificity varied for individual units, the population showed a strong bias for imagined reaches versus saccades (Student's t test, $P < 0.05$, Fig. 4D). Whereas some neurons showed a high degree of specificity for the left and right limb,

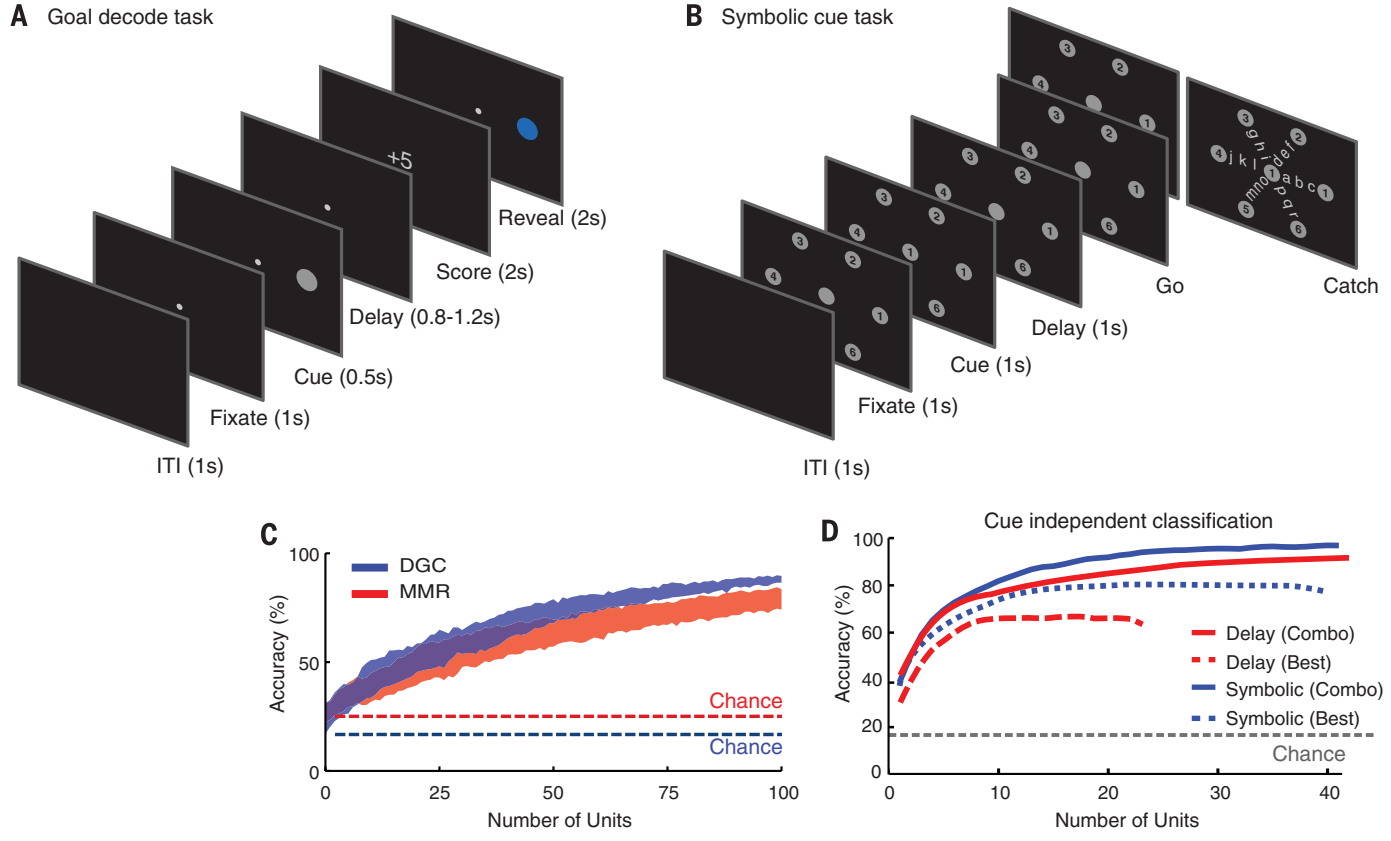

Fig. 3. Goal decoding. (**A**) Direct goal classification (DGC) task. EGS was instructed to intend motion toward a cued target through a delay period after the target was removed from the screen. Neural activity from the final 500 ms of the delay period was used to decode the location of the spatial target. EGS was awarded points depending on the relative location of the decoded and cued target. The decoded target location was presented at the end of each trial. (**B**) Symbolic task. A target grid was presented along with a number indicating the current target. The cue was removed during the delay period. A series of tones was used to cue the start and end of movements. Multiple effectors were tested in interleaved blocks. Catch trials provided a means to ensure that EGS was, on average, engaged in the task. (**C**) Estimated classification accuracy (mean with 95% CI) for variable population sizes. Populations were constructed by using randomly sampled units from the recorded population for the MMR and DGC tasks. Chance based on number of potential targets (MMR: four targets; DGC: six targets). (**D**) Greedy dropping curves show that high classification accuracy is possible whether targets are cued directly (A) or symbolically (B). Best: best single day performance; Combo: performance when combining data across days.

many reach-selective neurons were bimanual, as they frequently showed no bias for which limb EGS imagined using (Fig. 4E). The population response provided sufficient information to decode which effector EGS imagined using on a given trial (Fig. 4F).

The results show the coding of motor imagery in the human PPC at the level of single neurons and the encoding of goals and trajectories by populations of human PPC neurons. Moreover, many cells showed effector specificity, being active for imagining left-arm or right-arm movements or making actual eye movements. These results tie together NHP and human research and point to similar sensorimotor functions of the PPC in both species.

It could be argued that the results reflect visual attention rather than motor imagery. The voluntary activation of single neurons with specific imagined movements (e.g., movement of the hand to the mouth) without any visual stimulation argues against this sensory interpretation. The effector specificity also cannot be easily explained by a simple attention hypothesis.

The neural activity in delayed goal tasks is very similar to the persistent activity seen with planning in the NHP literature and attributed to the animals' intent (*14*). The PPC in NHPs codes both trajectory and goal information (*15*). The dynamics of this trajectory signal in NHPs, when compared to the kinematics of the co-occurring limb movements, suggest that the signal is a forward model of the limb movement; an internal monitor of the movement command in order to match the intended movement with actual movement for online correction (*15*). Deficits in online control in humans with PPC lesions have led investigators to propose that the PPC uses these forward models (*16*). If the trajectory signal is indeed a forward model, then EGS can generate this forward model through imagery without actually moving his limbs.

Effector specificity at the single-neuron level has been routinely reported in the PPC of NHPs (*17*). In NHPs, there is a map of intentions with areas selective for eye (lateral intraparietal area, LIP), limb (parietal reach region, PRR, and area 5d), and grasp (anterior intraparietal region, AIP) movements (*1*). Bimanual activity (left and right limb) from single PRR neurons has been reported with qualitatively similar results in the NHP (*18*). Control of two limbs across the spectrum of human behavior is challenging and requires both independent and coordinated movement between the limbs. One possibility is that units showing effector-specific and bimanual tuning could play complementary roles in independent and coordinated movements; however, more direct evidence in which EGS attempts various bimanual actions is necessary to fully test the potential for controlling two limbs from the PPC.

We have focused on the representation of motor intentions in the human PPC. Some cells appeared to code comparatively simple motor intentions, whereas others coded coordinated ethologically meaningful actions. One unexplored possibility is that the PPC also encodes nonmotor intentions such as the desire to turn on the television, or preheat the oven. As the world becomes increasingly connected through technology, the possibility of directly decoding nonmotor intentions to control one's environment may alter approaches to brain-machine interfaces (BMIs).

Neurons that constituted the recorded population would frequently change (fig. S2). This finding presents challenges for the widespread adoption of BMIs that can be addressed through a variety of techniques. One approach is the use of robust and adaptive decoding algorithms that can adapt alongside the changing neural population [e.g., (*19*)]. In the long term, the development of chronic recording technologies that can stably maintain recordings should be a priority.

This study shows that the human PPC can be a source of signals for neuroprosthetic applications in humans. The high-level cognitive aspects of movement imagery have several advantages for neuroprosthetics. The goal encoding can lead to very rapid readout of the intended movement (Fig. 2C). The PPC encodes both the goal and trajectory, which in NHPs improves decoding of movement goals when the two streams of information are combined in decoders (*10*). The bimanual representation of the limbs may allow the operation of two robotic limbs with recordings made from one hemisphere. In terms of usefulness for neuroprosthetics, it is difficult to directly compare the performance of PPC to previous studies of M1. In NHP studies, M1 has been shown to be a rich source of neural signals correlated with the trajectory of limb movements (*20*). In previous human M1 recordings, primarily the trajectory was decoded (*12*, *13*, *21*, *22*). The reported offline trajectory reconstructions from M1 populations are comparable to the values we achieved from PPC neurons (Fig. 2D) (*12*, *13*). The other aspects of encoding, e.g., goals and effectors, have not yet been examined in detail in human M1. However, it can be concluded from

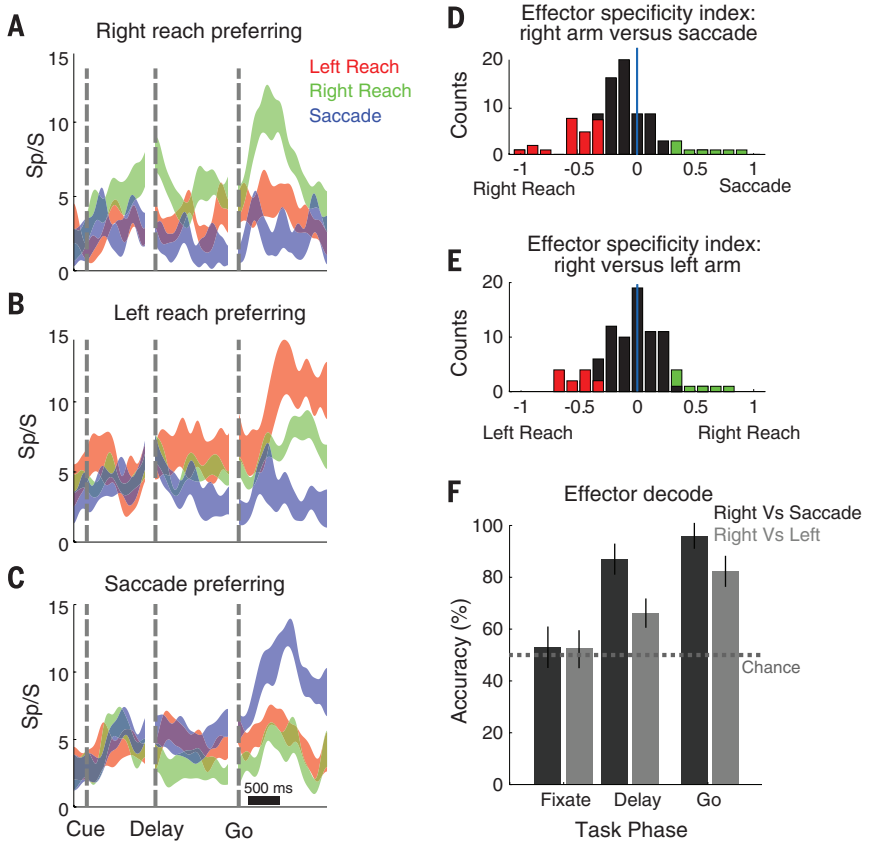

Fig. 4. Effector specificity in PPC. (**A**) Unit showing preferential activation to imagined movements of the right arm. Each trace shows the neural firing rate (mean ± SE) for the movement direction evoking the maximal response for each effector. (**B** and **C**) Same as (A), but for left arm and saccade-preferring neurons. (**D**) Population analysis. The degree of effector specificity varied across the population. Effector specificity was quantified with a specificity index based on the normalized depth of modulation (DM) for reaches versus saccades $\left(\frac{DM_{reach}-DM_{saccade}}{DM_{reach}+DM_{saccade}}\right)$. The specificity index for units that were spatially tuned to at least one effector is shown as a histogram. Colored bars indicate a significant preference for an effector. (**E**) Same as (D) but for imagined right arm versus left arm movements. (**F**) The effector used to perform the task could be decoded from the neural population (mean with 95% CI).

our study that the PPC is a good candidate for future clinical applications as it contains signals both overlapping and likely complementary to those found in M1.

REFERENCES AND NOTES

1. R. A. Andersen, C. A. Buneo, *Annu. Rev. Neurosci.* **25**, 189–220 (2002).
2. J. C. Culham, C. Cavina-Pratesi, A. Singhal, *Neuropsychologia* **44**, 2668–2684 (2006).
3. R. Balint, *Monatsschr. Psychiatr. Neurol.* **25**, 51–81 (1909).
4. M. T. Perenin, A. Vighetto, *Brain* **111**, 643–674 (1988).
5. M. A. Goodale, A. D. Milner, *Trends Neurosci.* **15**, 20–25 (1992).
6. A. Sirigu *et al.*, *Science* **273**, 1564–1568 (1996).
7. L. Pisella *et al.*, *Nat. Neurosci.* **3**, 729–736 (2000).
8. S. Musallam, B. D. Corneil, B. Greger, H. Scherberger, R. A. Andersen, *Science* **305**, 258–262 (2004).
9. M. Hauschild, G. H. Mulliken, I. Fineman, G. E. Loeb, R. A. Andersen, *Proc. Natl. Acad. Sci. U.S.A.* **109**, 17075–17080 (2012).
10. G. H. Mulliken, S. Musallam, R. A. Andersen, *J. Neurosci.* **28**, 12913–12926 (2008).
11. R. A. Andersen, S. Kellis, C. Klaes, T. Aflalo, *Curr. Biol.* **24**, R885–R897 (2014).
12. W. Truccolo, G. M. Friehs, J. P. Donoghue, L. R. Hochberg, *J. Neurosci.* **28**, 1163–1178 (2008).
13. S.-P. Kim, J. D. Simeral, L. R. Hochberg, J. P. Donoghue, M. J. Black, *J. Neural Eng.* **5**, 455–476 (2008).
14. J. W. Gnadt, R. A. Andersen, *Exp. Brain Res.* **70**, 216–220 (1988).
15. G. H. Mulliken, S. Musallam, R. A. Andersen, *Proc. Natl. Acad. Sci. U.S.A.* **105**, 8170–8177 (2008).
16. D. M. Wolpert, S. J. Goodbody, M. Husain, *Nat. Neurosci.* **1**, 529–533 (1998).
17. L. H. Snyder, A. P. Batista, R. A. Andersen, *Nature* **386**, 167–170 (1997).
18. S. W. C. Chang, A. R. Dickinson, L. H. Snyder, *J. Neurosci.* **28**, 6128–6140 (2008).
19. S. Dangi *et al.*, *Neural Comput.* **26**, 1811–1839 (2014).
20. A. P. Georgopoulos, J. F. Kalaska, R. Caminiti, J. T. Massey, *J. Neurosci.* **2**, 1527–1537 (1982).
21. L. R. Hochberg *et al.*, *Nature* **442**, 164–171 (2006).
22. J. L. Collinger *et al.*, *Lancet* **381**, 557–564 (2013).

ACKNOWLEDGMENTS

We thank EGS for his unwavering dedication and enthusiasm, which made this study possible. We acknowledge V. Shcherbatyuk for computer assistance; T. Yao, A. Berumen, and S. Oviedo, for administrative support; K. Durkin for nursing assistance; and our colleagues at the Applied Physics Laboratory at Johns Hopkins and at Blackrock Microsystems for technical support. This work was supported by the NIH under grants EY013337, EY015545, and P50 MH942581A; the Boswell Foundation; The Center for Neurorestoration at the University of Southern California; and Defense Department contract N66001-10-4056. All primary behavioral and neurophysiological data are archived in the Division of Biology and Biological Engineering at the California Institute of Technology.

SUPPLEMENTARY MATERIALS

www.sciencemag.org/content/348/6237/906/suppl/DC1
Materials and Methods
Figs. S1 to S3
Movies S1 to S3
References (*23*–*26*)

20 December 2014; accepted 31 March 2015
10.1126/science.aaa5417

EPIGENETICS

Multiplex single-cell profiling of chromatin accessibility by combinatorial cellular indexing

Darren A. Cusanovich,[1] Riza Daza,[1] Andrew Adey,[2] Hannah A. Pliner,[1] Lena Christiansen,[3] Kevin L. Gunderson,[3] Frank J. Steemers,[3] Cole Trapnell,[1] Jay Shendure[1]*

Technical advances have enabled the collection of genome and transcriptome data sets with single-cell resolution. However, single-cell characterization of the epigenome has remained challenging. Furthermore, because cells must be physically separated before biochemical processing, conventional single-cell preparatory methods scale linearly. We applied combinatorial cellular indexing to measure chromatin accessibility in thousands of single cells per assay, circumventing the need for compartmentalization of individual cells. We report chromatin accessibility profiles from more than 15,000 single cells and use these data to cluster cells on the basis of chromatin accessibility landscapes. We identify modules of coordinately regulated chromatin accessibility at the level of single cells both between and within cell types, with a scalable method that may accelerate progress toward a human cell atlas.

Chromatin state is dynamically regulated in a cell type–specific manner (*1*, *2*). To identify active regulatory regions, sequencing of deoxyribonuclease I (DNase I) digestion products [DNase-seq (*3*)] and assay for transposase-accessible chromatin using sequencing [ATAC-seq (*4*)] measure the degree to which specific regions of chromatin are accessible to regulatory factors. However, these assays measure an average of the chromatin states within a population of cells, masking heterogeneity between and within cell types.

[1]University of Washington, Department of Genome Sciences, Seattle, WA, USA. [2]Oregon Health and Science University, Department of Molecular and Medical Genetics, Portland, OR, USA. [3]Illumina, Inc., Advanced Research Group, San Diego, CA, USA.
***Corresponding author. E-mail: shendure@uw.edu**

Single-cell methods for genome sequence (*5*), transcriptomes (*6*–*10*), DNA methylation (*11*), and chromosome conformation (*12*) have been reported. However, we presently lack technologies for genome-wide, single-cell characterization of chromatin state. Furthermore, a limitation of most such methods is that single cells are individually compartmentalized, and the nucleic acid content of each cell is biochemically processed within its own reaction volume (*13*–*16*). Processing of large numbers of cells in this way can be expensive and labor intensive, and it is difficult to work with single cells, small volumes, and low nucleic acid inputs.

We recently used combinatorial indexing of genomic DNA fragments for haplotype resolution or de novo genome assembly (*17*, *18*). Here, we adapt the concept of combinatorial indexing to intact nuclei to acquire data from thousands of single cells without requiring their individualized processing (Fig. 1A). First, we molecularly barcode populations of nuclei in each of many wells. We then pool, dilute, and redistribute intact nuclei to a second set of wells, introduce a second barcode, and complete library construction. Because the overwhelming majority of nuclei pass through a unique combination of wells, they are "compartmentalized" by the unique barcode combination that they receive. The rate of "collisions"—i.e., nuclei coincidentally receiving the same combination of indexes—can be tuned by adjusting how many nuclei are distributed to the second set of wells (fig. S1) (*19*).

We sought to integrate combinatorial cellular indexing and ATAC-seq to measure chromatin accessibility in large numbers of single cells. In ATAC-seq, permeabilized nuclei are exposed to transposase loaded with sequencing adapters ["tagmentation" (*4*, *20*)]. In the context of chromatin, the transposase preferentially inserts adapters into nucleosome-free regions. These "open" regions are generally sites of regulatory activity and correlate with DNase I hypersensitive sites (DHSs).

In the integrated method, we molecularly tag nuclei in 96 wells with barcoded transposase complexes (Fig. 1A) (*17*–*19*). We then pool, dilute, and redistribute 15 to 25 nuclei to each of 96 wells of a second plate, using a cell sorter. After lysing nuclei, a second barcode is introduced during polymerase chain reaction (PCR) with indexed primers complementary to the transposase-introduced adapters. Finally, all PCR products are pooled and sequenced, with the expectation that most sequence reads bearing the same combination of barcodes will be derived from a single cell (estimated collision rate of ~11% for experiments described here) (fig. S1).

As an initial test, we mixed equal numbers of nuclei from human (GM12878) and mouse [Patski (*21*)] cell lines, performed combinatorial cellular indexing, and sequenced the resulting

Decoding motor imagery from the posterior parietal cortex of a tetraplegic human

Tyson Aflalo *et al.*

Science **348**, 906 (2015);
DOI: 10.1126/science.aaa5417